Title: Cysteine-rich receptor-like kinase and MADS-box co-regulation of programmed cell death drives apical spikelet degeneration in wheat

Qidi Du[1†], Zhengwu Fang[1†], Yongdun Xie[2], Hongchun Xiong[2], Linshu Zhao[2], Jiayu Gu[2], Huiyuan Li[2], Huijun Guo[2]*, Luxiang Liu[2]*

[1]MARA Key Laboratory of Sustainable Crop Production in the Middle Reaches of the Yangtze River (Co-construction By Ministry and Province) /Hubei Key Laboratory of Waterlogging Disaster and Agricultural Use of Wetland, College of Agriculture, Yangtze University, Jingzhou 434025, China

[2]State Key Laboratory of Crop Gene Resources and Breeding, National Engineering Laboratory of Crop Molecular Breeding, CAEA Research and Development Centre on Nuclear Technology Applications for Irradiation Mutation Breeding, Institute of Crop Sciences, Chinese Academy of Agricultural Sciences, Beijing 100081, China

*Corresponding authors: Luxiang Liu (liuluxiang@caas.cn), Huijun Guo (guohuijun@caas.cn)

† These authors contributed equally

The author responsible for distribution of materials integral to the findings presented in this article in accordance with the policy described in the Instructions for Authors (https://academic.oup.com/plphys/pages/General-Instructions) is Luxiang Liu

Short title: PCD-mediated wheat apical spikelet degeneration

Abstract: Spikelet degeneration and pollen sterility are primary constraints on grain set in wheat (*Triticum aestivum* L.), yet their molecular underpinnings remain poorly defined. We characterized *degenerated spikelets 1* (*ds1*), a wheat mutant displaying apical spikelet degeneration and middle spikelet sterility. Relative to wild type (WT), *ds1* exhibited a 17.0% reduction in spike length, an 88.8% decline in grain-bearing spikelets, and a 93.6% drop in grain number per spike. Fine mapping localized the causal locus to chromosome 3BL, where *DS1*, encoding a cysteine-rich receptor-like kinase (CRK), was identified as the causal gene and found to be strongly down-regulated in degenerated spikelets. Concordantly, multiple MADS-box transcription factors were transcriptionally suppressed in *ds1* degenerated spikelets. Histological analysis revealed anther shrinkage, disrupted boundaries between anther wall layers, and defective cuticle structure. Excessive reactive oxygen species (ROS) accumulated in the anther outer wall, triggering programmed cell death (PCD). Loss of cuticular wax on the anther surface, combined with premature tapetal degradation, produced hollow anther locules, aberrant pollen exine layering, and failure of microspore maturation, culminating in sterility. Together, these findings demonstrate that coordinated regulation of PCD, tapetal development, and pollen exine formation is indispensable for normal spikelet and floret development in wheat.

Keywords: wheat, degenerated spikelet, anther and pollen defects, protein kinases, MADS-box

Introduction

Spikelets are the fundamental developmental units of Poaceae inflorescences, and their differentiation and branching architecture directly determine grain yield (Backhaus et al., 2022). Although emergence of the apical spikelet marks the completion of spikelet differentiation, not every inflorescence meristem successfully transitions into a spikelet meristem. Physiological and environmental perturbations frequently prevent apical and basal spikelets from developing into grains (Heng et al., 2018; Zafar et al., 2020). In wheat, spikelet number and floret fertility jointly govern grain set per spike and, ultimately, yield, making the molecular genetic basis of spikelet and floret development a central question in crop improvement.

Mutants with apical spikelet defects have been well characterized in rice. *dps1* displays apical spikelet degeneration, reduced middle spikelet fertility, altered anther cuticle morphology, and reactive oxygen species (ROS) induced programmed cell death (PCD) (Zafar et al., 2020). ROS accumulation in *spl6-1* similarly drives apical spikelet degeneration, producing a characteristic bare-tip phenotype (Wang et al., 2018), while *tut1* combines apical spikelet degeneration with elevated ROS and anther-pollen developmental defects (Bai et al., 2015). In *paab1-1*, degenerating spikelets undergo PCD accompanied by marked H_2O_2 accumulation (Heng et al., 2018), and defective apical anther cuticle formation in *apa1331* causes anther degeneration (Ali et al., 2022). Across these rice mutants, ROS imbalance and PCD activation emerge as recurrent themes in apical spikelet degeneration. In wheat, key regulators of spikelet meristem identity and floral transition have been cloned or mapped, including *VRN1*, *FUL2* (Li et al., 2019), *WPS1*

(Zhang et al., 2022a), *WFZP* (Li et al., 2020; Du et al., 2021), *TaAGL6* (Kong et al., 2022), *TaCol-B5* (Zhang et al., 2022b), *TaSus1* (Shen et al., 2024), *TaeEF1A* (Yan et al., 2025), and *TaWUS-D1* (Tian et al., 2025). Notably, SQUAMOSA and SVP family MADS-box proteins act synergistically during apical meristem transition yet antagonistically during the spikelet meristem to floral organ transition (Li et al., 2021). Despite substantial progress in understanding spike architecture and floral organ identity, the molecular mechanisms governing spikelet degeneration, particularly at the spike apex, remain largely unexplored.

Pollen development is a critical determinant of reproductive success in flowering plants, encompassing a sequence of tightly coordinated events from anther morphogenesis to mature pollen release (Huo et al., 2020). Central among these is tapetal PCD, which is initiated following meiosis of microspore mother cells (Xie et al., 2014). The tapetum, as the innermost anther wall layer, serves as both the nutritive and regulatory hub of pollen development; premature or delayed tapetal PCD invariably results in pollen abortion (Niu et al., 2013; Bai et al., 2019; Liu et al., 2021a). Key regulators of tapetal PCD include *OsAPI5*, *TIP2*, *TDR*, and *EAT1* (Lee et al., 2004; Li et al., 2006; Li et al., 2011; Niu et al., 2013; Ko et al., 2014). ROS, as a pivotal PCD signaling molecule, disrupts redox balance when excessively accumulated. In multiple species, aberrant ROS levels are directly linked to premature tapetal degradation and resultant sterility; *Ms2*, *ADT1*, *ZmENR1*, and *RBOHE* all impair redox homeostasis through ROS dysregulation, causing aberrant tapetal PCD timing (Xie et al., 2014; Ni et al., 2017; Liu et al., 2022a; Liu et al., 2024; Zhan et al., 2024). Beyond tapetal function, the pollen exine, synthesized by the tapetum, shields developing pollen from biotic and abiotic stresses (Shi et al., 2015; Tao et al., 2021; Yuan et al., 2022), and exine defects cause pollen abortion across species. In rice, *OsABCG26*, *PDA1*, *OsC6*, *OsLTP47*, *RMS2*, *OsGELP110*, *OsGELP115*, and *OsGPT1* have all

been implicated in pollen fertility through their roles in exine formation (Zhang et al., 2010; Qin et al., 2013; Zhao et al., 2015; Chang et al., 2016; Zhang et al., 2020; Zhao et al., 2020; Zhang et al., 2021b; Chen et al., 2022). In wheat, the orthologous gene *TaMs1* similarly disrupts pollen exine architecture, causing complete male sterility (Tucker et al., 2017; Kouidri et al., 2018), though the repertoire of characterized wheat exine genes remains limited.

Receptor-like kinases (RLKs) are indispensable regulators of spikelet development, operating through complex signal transduction networks. Leucine-rich repeat RLKs (LRR-RLKs) and mitogen-activated protein kinases (MAPKs) have established roles in spike and floral organ development: *OsMSP1*, *FON1*, and *OsERL* regulate floral organ development (Nonomura et al., 2003; Suzaki et al., 2004; Yang et al., 2016; Liu et al., 2021b; Han et al., 2023), while *AtMPK3*, *AtMPK6*, and *ERECTA* (*ER*) control cell proliferation and differentiation during anther development (Bush and Krysan, 2007; Hord et al., 2008). The *OsER1–OsMKKK10–OsMKK4–OsMPK6* cascade governs rice inflorescence formation (Shen et al., 2015; Guo et al., 2020), and *OsYDA1/OsYDA2–OsMKK4–OsMPK6* is required for tapetal development and male gametogenesis (Zeng et al., 2024). Cysteine-rich receptor-like kinases (CRKs), a distinct RLK subfamily, regulate Ca^{2+} influx, ROS homeostasis, MAPK cascade activation, and callose deposition (Zhang et al., 2023). CRKs have also been linked to inflorescence development: the *Arabidopsis crk10-A397T* mutant exhibits impaired inflorescence development and apical meristem degeneration (Piovesana et al., 2023). Despite the well-defined roles of RLKs in model plant reproductive development, whether CRKs participate in wheat spikelet development remains unknown.

Here, we characterize *ds1*, a wheat mutant with degenerated apical spikelets and sterile middle spikelets driven by ROS-induced PCD. Tapetal degradation, cuticular dysplasia, and disrupted

pollen exine stratification collectively yield shrunken, non-viable pollen grains. The *ds1* is mapped to a single dominant locus on chromosome 3BL, where the candidate gene *DS1* encodes a CRK that is down-regulated in degenerated spikelets and appears to modulate spike development through transcriptional control of MADS-box genes. This study clarifies the developmental basis of apical and middle spikelet failure in wheat and implicates CRK-mediated signaling as a regulator of spikelet development.

Results

Apical spikelet degeneration in *ds1* compromises agronomic performance

The apical spikelets of *ds1* degenerated conspicuously, and a subset of spikes failed to emerge from the flag leaf (Figure 1A and B). The statistical results of agronomic traits revealed a 17.0% reduction in spike length, an 88.8% decline in grain-bearing spikelet number, and a 93.6% drop in grains per spike (Supplemental Figure 1A–C). Grain length increased by 9.1% in *ds1*, whereas grain width and thousand-grain weight were unchanged relative to WT (Supplemental Figure 1D–G). Plant height was reduced by 48.3% (Supplemental Figure 1H).

To identify when degeneration initiates, we tracked apical spikelet development from the spike meristem stage onward. At the single-ridge stage, the earliest phase of spike development and the onset of vegetative-to-reproductive transition, no morphological differences were detectable between *ds1* and WT (Figure 1C; Supplemental Figure 2A and B). By the tetrad stage, however, apical spikelets of *ds1* lagged markedly in growth rate and were significantly shorter than those of WT, while middle spikelets remained unaffected (Figure 1C; Supplemental Figure 2C and D). Degeneration of the apical spikelets was clearly evident from the tetrad stage onward; by late uninucleate stage, *ds1* apical spikelets appeared white and stunted (Figure 1D and E), with length

significantly below that of WT (Supplemental Figure 2E). Thus, apical spikelet degeneration in *ds1* is initiated during early spikelet development and culminates in structurally incomplete spikelets at maturity.

ROS-driven redox imbalance underlies *ds1* sterility

Anthers of *ds1* apical spikelets were shrunken and progressively dried to a translucent state, diverging from WT in appearance at an early developmental stage (Figure 2A–C). Middle spikelet anthers of *ds1* appeared yellowish, consistent with PCD-associated changes. I_2-KI staining confirmed that pollen from both apical and middle spikelets of *ds1* was non-viable, and apical spikelet pollen was not released from the anthers (Figure 2D–F).

ROS accumulation was assessed by 3,3'-diaminobenzidine (DAB) and nitroblue tetrazolium (NBT) staining, which detect peroxidase activity via insoluble brown precipitate and superoxide anion (O_2^-) via blue formazan, respectively. DAB staining revealed intense brown coloration in both apical and middle spikelet anthers of *ds1*, indicative of peroxidase accumulation in sterile anthers (Figure 2G). NBT staining corroborated O_2^- accumulation in the same tissues (Figure 2H). Superoxide dismutase (SOD) activity, the primary enzymatic scavenger of O_2^-, and malondialdehyde (MDA) content, a marker of membrane lipid peroxidation, were both elevated in degenerated and sterile anthers of *ds1*, confirming a ROS burst (Figure 2I and J). Correspondingly, respiratory burst oxidase homolog, glutathione peroxidase, and peroxidase, critical components of ROS metabolism, exhibited systemic transcriptional dysregulation in the degenerated spikelets (Supplemental Figure 3). This disruption collectively tipped the redox balance, converting ROS from signals to cytotoxic effectors, which ultimately drove PCD in the spikelets.

Cuticular dysplasia impairs anther fertility

The anther cuticle is a critical lipid barrier that protects developing male gametes from environmental stresses and is required for normal pollen development (Shi et al., 2015; Liu et al., 2022b). At the mature pollen stage, WT anther surfaces were uniformly covered with wax and displayed a characteristic reticulate structure (Figure 3A and B). In *ds1* middle spikelet anthers, a striated surface pattern was present but the wax architecture was noticeably looser (Figure 3C and D). Apical spikelet anthers of *ds1* lacked any discernible wax structure entirely, instead presenting a smooth, featureless surface (Figure 3E and F), suggesting that defective cuticle development contributes directly to reduced floret fertility.

Scanning electron microscopy (SEM) revealed that *ds1* pollen grains were shrunken and collapsed, in stark contrast to the plump, well-developed grains of WT. Apical spikelet pollen was more severely shriveled than middle spikelet pollen (Figure 3G–L; Supplemental Figure 4A–F). The germination apertures of *ds1* sterile pollen were compressed and distorted, and the pollen exine projections were denser and sharper than those of WT spreading pollen (Figure 3M–O; Supplemental Figure 4G–I). Ubisch bodies, tapetum-specific structures that transport sporopollenin precursors to the microspore surface (Shi et al., 2015), were clumped in *ds1*, failing to adopt the reticulate organization seen in WT (Figure 3P–R). This aberrant Ubisch body morphology likely reflects defective tapetal development during the sporogenous period, which compromises the production of normal sporopollenin precursors.

Premature tapetal degradation and pollen exine abnormalities drive *ds1* sterility

To dissect the structural basis of *ds1* sterility, we examined anther cross-sections and pollen ultrastructure by light microscopy and transmission electron microscopy (TEM). At the early

uninucleate stage, WT anthers displayed the canonical four-layered wall architecture, including epidermis, endothecium, middle layer, and tapetum, in regular arrangement (Figure 4A). *ds1* sterile anthers, by contrast, had an irregularly elliptical cross-sectional profile with disordered wall layering (Figure 4E; Supplemental Figure 4J–L). In WT, tapetal thinning commenced at the late uninucleate stage, marking the onset of developmentally programmed degradation, with microspores entering the vacuolate state (Figure 4B); tapetal remnants persisted through the binucleate stage before near-complete degradation by the trinucleate stage (Figure 4C and D). In *ds1* sterile anthers, the epidermis expanded abnormally from the early uninucleate stage onward, compressing and rupturing the inner layers throughout development (Figure 4E–H). Tapetal degradation in sterile anthers had already disappeared at the binucleate stage, likely depriving microspores of the metabolic support required for maturation and impairing fertilization (Figure 4G). No mature pollen grains formed in sterile anthers; only undeveloped microspores were observed. Anthers from degenerated *ds1* spikelets were still more severely affected, with poorly defined wall layers and hollow microspores compressed against one another (Figure 4I–K; Supplemental Figure 4M–O). TEM confirmed premature tapetal degradation in *ds1* sterile florets, with the epidermis, endothecium, and middle layer all showing variable degrees of collapse (Figure 4L–Q). Pollen grains from *ds1* were desiccated and irregular, devoid of starch or other storage materials evident in WT grains (Figure 4R–T), consistent with the absence of brown I_2-KI staining in sterile pollen (Figure 2D–F). Statistical analysis confirmed that all WT pollen grains were round and starch-filled, whereas all *ds1* pollen grains from both apical and middle spikelets were irregular and hollow (Supplemental Figure 5A).

Pollen exine, composed primarily of sporopollenin synthesized and secreted by the tapetum (Ariizumi and Toriyama, 2011; Hou et al., 2023), consists of nexine, baculum, tectum, and

microchannels. In *ds1* sterile anthers, pollen exine was markedly thickened relative to fertile anthers, yielding a disproportionate intine-to-exine ratio (Figure 4U–W; Supplemental Figure 4M–O). At the trinucleate stage, nexine, tectum, and total exine thickness in *ds1* apical spikelets were increased by 46.5%, 65.2%, and 52.7%, respectively, and in middle spikelets by 64.3%, 40.4%, and 46.0%, respectively (Supplemental Figure 5B–D). Furthermore, bacula collapsed into spherical forms and could no longer bridge the tectum to the nexine. These exine abnormalities likely reflect an inability to supply appropriate sporopollenin precursors and metabolites for pollen maturation. Taken together, premature tapetal degradation and defective pollen exine development are the proximal causes of sterility in *ds1*.

_DS1_ encodes a cysteine-rich receptor-like kinase

F_1 plants derived from crosses between *ds1* and WT displayed degenerated apical spikelets and sterile middle florets (Supplemental Figure 6A and B), recapitulating the *ds1* phenotype. In the F_2 population from a cross between *ds1* and cultivar Zhongmai175, degenerate and normal plants segregated at a 3:1 ratio (Supplemental Table 1; Supplemental Figure 6C), establishing that the *ds1* phenotype is conditioned by a single dominant gene.

Exon capture sequencing identified a tightly linked genomic interval at the distal end of chromosome 3BL, with SNPs enriched within the 800–830 Mb region (Supplemental Figure 7). Molecular marker-based linkage analysis delimited the locus to a 3BL interval flanked by markers M11 and M12 (Figure 5A; Supplemental Table 2), and six independent recombinants were isolated. All six exhibited degenerated apical spikelets, whereas their plant height, heading date, and tiller number remained comparable to those of the WT (Supplemental Figure 8), this indicates that the mapped interval specifically regulates spikelet development without pleiotropic effects on other agronomic traits. Within this interval, the Chinese Spring reference genome

(IWGSC RefSeq v2.1) contains seven high-confidence genes: one encoding a ribonuclease P protein (*TraesCS3B03G1383000*) and six encoding CRKs (Supplemental Table 3). Sequence analysis of all seven genes and their promoters revealed a mutation exclusively in *TraesCS3B03G1384200*. Expression profiling further showed that only *TraesCS3B03G1383800* and *TraesCS3B03G1384200* were significantly down-regulated in *ds1*, with the remaining five genes barely expressed (Figure 5B). We further detected tissue expression patterns of *TraesCS3B03G1384200*, and except for the apical spikelets, there was no significant difference in basal spikelets, stems or leaves (Figure 5C). Based on the coincident sequence mutation and transcriptional downregulation, we designated *TraesCS3B03G1384200* as the candidate gene *DS1*.

DS1 encodes a CRK comprising two GNK2 domains and a protein kinase domain, with 94.43% amino acid sequence identity to the previously characterized cysteine-rich receptor-like protein kinase 10 isoform X2 from *Triticum urartu* (Supplemental Table 4). The *ds1* mutation, a C506T missense substitution, falls at the front end of the second GNK2 domain and converts Threonine (Thr) to Isoleucine (Ile) at residue 169 (Figure 5D). This residue resides on an α-helix and constitutes a predicted phosphorylation site: the phosphorylation potential score of Thr169 reached 0.611, indicating a high probability of phosphorylation (Supplemental Figure 9A–C). The Thr169Ile substitution abolishes this phosphorylation capacity, since the hydroxyl group of Thr, which accepts phosphate groups, is replaced by the non-phosphorylatable hydrophobic side chain of Ile. Beyond the loss of phosphorylation, the substitution likely disrupts the local hydrogen-bond network and conformational integrity required for kinase activation (Supplemental Figure 9A and B). Transmembrane helix prediction indicated that residues 315–337 form a confirmed transmembrane helix, while residues 13–35 and 147–169 exhibit sub-

threshold transmembrane helix propensity (Supplemental Figure 10A and B). Notably, the Thr169Ile mutation falls within the second potential transmembrane region and raises the prediction score, suggesting the substitution increases the likelihood of this segment forming a transmembrane helix (Supplemental Figure 10A and B).

To validate *TraesCS3B03G1384200* as the gene controlling spikelet degeneration, we identified four independent allelic mutants derived from Jing411 or Fielder background, all of them phenocopied *ds1* (Figure 5D and E). *je0428* carries a G1092A mutation causing premature translation termination at position 364, while *e0920* carries a C1819T mutation terminating translation at position 607 (Figure 5D; Supplemental Figure 11A and B), *F-868* carries a C853T mutation terminating translation at position 285 (Figure 5E; Supplemental Figure 11D). The three nonsense alleles produced apical spikelet degeneration with sterile anthers beneath the degenerated spikelets (Figure 5D and E). Grain-bearing spikelet numbers was declined by 48.0% in *je0428*, 36.1% in *e0920* and 39.2% in *F-686*, and seed setting rate was reduced by 55.7%, 33.9% and 45.7%, respectively (Figure 5F-I; Supplemental Figure 12). It was remarkable that we identified an independent heterozygous allelic mutant, *F-854*, of *TraesCS3B03G1384200* from a Fielder mutant resource (Figure 5E). *F-854* carries a C586T missense mutation (Supplemental Figure 11C), resulting in an amino acid substitution from Proline (Pro) to Serine (Ser) at residue 196, and its offspring carrying alleles TT ($F\text{-}854^{TT}$) or CT ($F\text{-}854^{CT}$) exhibited a phenotype identical to *ds1*, while those carrying allele CC ($F\text{-}854^{CC}$) produced a phenotype identical to its wild type Fielder (Figure 5E), this eliminates the possibility that other background mutations contribute to the phenotype. We observed in two different genetic backgrounds, mutations of gene *TraesCS3B03G1384200* resulted in apical spikelet degeneration and reduced middle

spikelet fertility. These converging lines of genetic and molecular evidence confirm *TraesCS3B03G1384200* as the causal gene underlying wheat apical spikelet degeneration.

MADS-box transcription factors regulate and affect spikelet development

To investigate how DS1 governs spikelet and floret development, we performed RNA-seq on young apical spikelets from *ds1* and WT at three developmental stages, focusing differential expression analysis on the floral organ primordia differentiation stage and late uninucleate stage. Post-translational modification pathways were prominently enriched among differentially expressed genes (Supplemental Figure 13A and B). Given that phosphorylation is the most prevalent post-translational modification and that *DS1* encodes a kinase, we examined the 148 differentially expressed genes mapping to phosphorylation-related pathways (Supplemental Table 5). Of these, 96 were differentially expressed exclusively at the late uninucleate stage, not at the floral organ primordia differentiation stage, a temporal pattern closely mirroring the onset of spikelet degeneration in *ds1*. This stage-specific enrichment implicates aberrant protein phosphorylation may be a significant contributor to the degeneration phenotype.

DNA-binding activity was also significantly enriched among differentially expressed genes (Supplemental Figure 13C), with MADS-box transcription factors standing out as a prominently dysregulated group in *ds1* apical spikelets (Figure 6A; Supplemental Table 6). Expression of 36 MADS-box genes showed no significant difference between WT and *ds1* at the floral organ primordia differentiation stage, but strong differential expression emerged by the late uninucleate stage, a temporal pattern again coinciding precisely with visible spikelet degeneration. RT-qPCR confirmed significant down-regulation of 10 MADS-box genes in *ds1* degenerated spikelets, with *MADS4*, *MADS7*, and *MADS22* showing the highest expression levels in WT (Figure 6B). These *MADS-box* genes exhibited eigengene-based connectivity (kME) values greater than 0.9 in

a spike development-related module identified by weighted gene co-expression network analysis (WGCNA), indicating that they are closely associated with the spike development process (Figure 6C; Supplemental Table 7). Furthermore, the expression pattern of *MADS22* in the recombinant lines was consistent with parents, whereas the expression patterns of *MADS4* and *MADS7* differed from parents (Figure 6D). These results indicate that DS1 regulates the transcriptional output of MADS-box factors through its regulatory relationship with MADS genes, that this regulatory relationship is inherited in the progeny.

Discussion

PCD underlie apical spikelet degeneration in *ds1*

ROS functions as a key signaling molecule governing cell fate during spikelet development, and its excessive accumulation is a well-documented trigger of aberrant PCD leading to spikelet degeneration. In *dps1* and *apa1331*, ROS accumulation intensifies PCD and drives spikelet degeneration (Zafar et al., 2020; Ali et al., 2022), while apical spikelet degeneration in *paab1-1* and *spl6-1* is likewise accompanied by PCD at later spike developmental stages, producing the characteristic bare-tip phenotype (Heng et al., 2018; Wang et al., 2018). Beyond genetic perturbation, high-temperature stress in maize disrupts endoplasmic reticulum function, elevates ROS, and suppresses spike development, reducing grain number (Wang et al., 2025). In *ds1*, apical spikelet development was already lagging at the tetrad stage, and this delay escalated into overt degeneration. ROS burst, and elevated MDA levels in the degenerated spikelets confirmed intracellular redox imbalance, placing *ds1* within a conserved mechanistic framework in which PCD-mediated apical spikelet degeneration, well-documented in rice, extends to wheat.

Premature tapetal PCD and pollen exine defects underlies *ds1* sterility

The tapetum is the primary source of nutrients and structural precursors for pollen exine formation and microspore maturation, and the precise timing of tapetal PCD is indispensable for fertility; both premature and delayed PCD result in pollen abortion (Xu et al., 2014; Gómez et al., 2015; Yang et al., 2019). Delayed tapetal PCD in *tdr*, *eat1*, *dtc1*, and *osedm2l* disrupts anther development and impairs fertility (Li et al., 2006; Ji et al., 2013; Niu et al., 2013; Yi et al., 2016; Ma et al., 2021), while the *ospdt1* mutant illustrates the opposite extreme, with premature tapetal PCD producing disordered pollen walls and aborted pollen (Yin et al., 2022). In *ds1*, the anther wall layer boundaries were blurred, tapetal degradation was premature, and hollow microspores failed to develop into mature pollen. Ubisch bodies, tapetum-specific structures that deliver sporopollenin precursors to the microspore surface (Tao et al., 2021), were clumped in *ds1*, failing to form the interconnected network present in WT. Taken with our ROS measurements, these observations are consistent with ROS-regulated tapetal degradation and its downstream consequences for fertility.

Because pollen exine assembly is primarily orchestrated by the tapetum (Zhou et al., 2015), tapetal abnormalities predictably disrupt exine architecture. In *ptc1*, *ipe2*, and *ms-6007*, delayed tapetal PCD produces malformed pollen walls and sterility (Li et al., 2011; Huo et al., 2020; An et al., 2020). In *ds1*, defective tapetal development similarly disorganized pollen exine stratification, producing disproportionate layer ratios and reduced fertility. The regulatory network controlling pollen exine formation is increasingly well characterized in rice and other cereals, but equivalent studies in wheat remain limited, underscoring the need for further investigation in this crop.

CRK-mediated kinase signaling in wheat spikelet development

RLKs mediate plant cell–cell communication (Zhu et al., 2024), and substantial evidence supports roles for LRR-RLKs and MAPKs in intercellular signaling during reproductive development (Yang et al., 2003; Hord et al., 2008; Peng et al., 2018; Zeng et al., 2024). Yet the contribution of CRKs to wheat spikelet development has remained unexplored. Loss of *Arabidopsis CRK10* function causes apical meristem degeneration (Piovesana et al., 2023), and the present work shows that DS1, a CRK highly homologous to CRK10 isoform X2 from *Triticum urartu*, controls spikelet development in wheat. DS1 is distinct from TaCRK10, previously identified in the common wheat variety Xiaoyan6 (Wang et al., 2021), which is instead highly homologous to CRK10 from *Aegilops tauschii* subsp. *tauschii* and shares low sequence similarity with DS1. Although their phosphorylase kinase domains are conserved, their GNK2 domains and transmembrane sequences diverge considerably, likely underlie their functional divergence. Unlike DS1, TaCRK10 confers stripe rust resistance and has no apparent role in spikelet development (Wang et al., 2021).

In canonical RLK architecture, an extracellular N-terminal domain perceives signals, a transmembrane domain anchors the protein at the membrane, and a cytoplasmic kinase domain phosphorylates downstream targets (Zhu et al., 2024). The transmembrane domain is particularly important for CRK subcellular localization (Zhang et al., 2023). The Thr169Ile substitution in DS1 falls within the second potential transmembrane region and elevates its helix-formation propensity above the prediction threshold, raising the possibility that this mutation alters DS1 subcellular localization, a hypothesis requiring experimental validation. More broadly, whether Thr169 is itself a phosphorylation site, and whether the DS1 kinase domain phosphorylates specific downstream substrates, remain open questions. Also notable is that the five genes upstream of *DS1* in the locus likewise encode CRKs, forming a gene cluster.

TraesCS3B03G1383800 among these is significantly down-regulated in *ds1*, raising the possibility that it forms a functional complex with DS1 to co-regulate spikelet development, though this awaits direct testing. The remaining cluster members showed negligible expression in apical spikelets, making their involvement at this developmental stage unlikely.

ds1 may modulate spikelet development through MADS-box transcription factors

In the ABCDE model of floral organ identity, nearly all key regulators are MIKC-type MADS-box transcription factors, with AP2 as the sole exception (Callens et al., 2018; Chongloi et al., 2019; Schilling et al., 2020; Kong et al., 2022). OsMADS4 interacts with SPW1 to specify lodicule and stamen identity (Yao et al., 2008; Duan et al., 2012), and HvMADS4-deficient barley exhibits homeotic stamen-to-pistil conversion producing supernumerary ovaries, phenotypically resembling the *multiple ovaries 3.h* mutant (Sun et al., 2024). Simultaneous down-regulation of *OsMADS7* and *OsMADS8* causes aberrant floral morphology and loss of floral determinacy (Cui et al., 2010; Zhang et al., 2018), while OsMADS22 promotes reproductive development by influencing spikelet meristem differentiation and floret morphogenesis (Sentoku et al., 2005; Fornara et al., 2008; Lee et al., 2008). In *ds1*, ten MADS-box transcription factors were significantly down-regulated in degenerated apical spikelets relative to WT. Given that the expression pattern of *MADS22* in the recombinant lines is consistent with their parents, its suppression likely contributes substantially to the apical spikelet degeneration phenotype. Whether DS1 directly controls their transcription or acts through intermediary factors remains to be determined.

Conclusion

We characterized a wheat mutant combining apical spikelet degeneration with middle floret sterility. Apical spikelet development was delayed from the tetrad stage onward, culminating in degeneration, while premature tapetal PCD and disrupted pollen exine formation drove middle floret sterility. Genetic analysis mapped the dominant causal locus to chromosome 3BL, where *DS1* (*TraesCS3B03G1384200*) encodes a CRK. A missense Thr-to-Ile substitution in DS1 coincided with marked transcriptional down-regulation of the gene in the mutant. Downstream, *DS1* loss of function suppressed multiple MADS-box transcription factors, implicating a CRK–MADS-box regulatory axis in the control of wheat spikelet development. These findings advance our mechanistic understanding of apical spikelet development and identify *DS1* as a candidate for improving grain number in wheat.

Materials and methods

Plant materials and growth conditions

The *ds1* mutant was isolated from an ethyl methane sulfonate (EMS)-mutagenized population of Jing411 (WT) (Guo et al., 2017) and advanced to the M_6 generation by selfing prior to this study. WT and *ds1* were each grown in four-row plots for phenotypic variation of the mutant. The F_2 mapping population was derived from a *ds1*×Zhongmai175 cross; 356 F_2 individuals were used for preliminary mapping and 1,604 for fine mapping. Each F_2 plant was selfed to F_3 for phenotypic confirmation. All plants were grown under standard management at the experimental station of the Institute of Crop Sciences, Chinese Academy of Agricultural Sciences, Beijing, with 2 m row length and 20 seeds per row.

Agronomic trait assessment

At maturity, 20 plants of comparable growth vigor were randomly selected from *ds1* and WT. Plant height was measured along the main stem from ground level to the spike apex (awns excluded), and main spike length was measured from the basal to the apical spikelet. Only spikelets bearing at least one grain were counted; empty spikelets were excluded. Grains were threshed per main spike and counted individually. Grain length, grain width, and thousand-grain weight were determined using an automated seed phenotyping system (WSeen Detection Technology, China).

Spikelet characterization

Spike development was tracked from the single-ridge stage through the early uninucleate stage using an Olympus SZX16 stereomicroscope (Olympus, Japan). Spike length and apical and middle spikelet lengths were measured at single-ridge stage and tetrad stage with three biological replicates per time point.

For anther sectioning, fresh anthers were collected at the early uninucleate, late uninucleate, binucleate, and trinucleate stages, with three anthers from different spikes per stage as biological replicates. Anthers were fixed immediately in formalin–acetic acid–alcohol (FAA) solution (50% ethanol) under vacuum, dehydrated through an ethanol series (70%, 80%, 90%, 95%, and 100%, 40 min each), and embedded in resin. Ultrathin sections were cut on a Leica EMUC7 microtome (Leica, Germany), stained with toluidine blue, and imaged on a Zeiss Axio Imager 2 (ZEISS, Germany), with four sections per anther.

Pollen viability was assessed by I_2-KI staining. Anthers were placed on slides, stained with a drop of I_2-KI solution, covered with a coverslip, and gently tapped to release pollen. Observations were made under a light microscope with three biological replicates per stage.

Electron microscopic observation

Anthers collected at the uninucleate and trinucleate stages from WT and *ds1* respectively, with one anther per spikelet, were processed for either SEM or TEM observation.

For SEM, anthers were fixed in FAA (50% ethanol) under vacuum and stored in fixative for at least 24 hours. Samples were dehydrated through a graded ethanol series (30%, 50%, 70%, 80%, 95%, and 100%), and the tissues were then dried using a CO_2 critical point dryer EM CPD300 (Leica, Germany). Dried samples were examined on a CIQTEK SEM5000 scanning electron microscope (CIQTEK, China), with three biological replicates per stage.

For TEM, anthers were fixed in 2.5% glutaraldehyde, rinsed with 0.1 M PBS, and post-fixed in OsO_4. Following gradient ethanol dehydration and resin embedding, ultrathin transverse sections were cut and examined on a Hitachi HT7700 transmission electron microscope (Hitachi, Japan). Three anthers were sectioned per stage (five sections each), and exine, tectum, and nexine thicknesses were measured in five random fields of view with two technical replicates.

Histochemical ROS detection

ROS accumulation was visualized by DAB and NBT staining at the binucleate stage, with three biological replicates per genotype. For DAB staining, anthers were vacuum-infiltrated at -0.1 MPa for 30 minutes in 1 mg/mL DAB (pH 3.8; Coolaber, China), then incubated in darkness at room temperature for 12 hours. Background pigment was removed by incubation in 95% ethanol at 80°C until the solution ran clear. Brown precipitate indicated H_2O_2 accumulation. For NBT staining, anthers were vacuum-infiltrated in 0.1% NBT (pH 7.8; Coolaber, China) at -0.1 MPa for 30 minutes, incubated in darkness for 2 hours, then destained in 95% ethanol at 80°C. Blue

formazan precipitate indicated O_2^- accumulation. Stained anthers were documented under a stereomicroscope.

SOD activity and MDA content detection

Fresh anthers from WT and *ds1* were collected at the binucleate stage, ground to fine powder in pre-cooled mortars, and 100 mg aliquots per sample were used for SOD and MDA assays, each with three biological and four technical replicates.

SOD activity was measured using a Solarbio microassay kit (Solarbio, China). Tissue was homogenized in 1 mL extraction buffer, centrifuged at 8,000×*g* at 4°C for 10 minutes, and the supernatant collected on ice. Enzyme and Water-Soluble Tetrazolium-1 working solutions were added per the manufacturer's protocol, incubated at 37 °C for 20 minutes, and absorbance measured at 450 nm. SOD activity (U/g) was calculated as: [inhibitory rate / (1- inhibitory rate) × V1] / (W × V2 / V3) × F. Inhibitory rate = $(\Delta A_{blank} - \Delta A_{determination}) / \Delta A_{blank} \times 100\%$.

MDA content was measured using a Solarbio microassay kit (Solarbio, China). Tissue (100 mg) was lysed in 1 mL cell lysis buffer and centrifuged to collect supernatant. MDA assay working solution was added to the supernatant, incubated at 100 °C for 15 minutes, and absorbance measured at 532 nm and 600 nm. MDA content (nmol/g) was calculated as: $[\Delta A \times V_1 / (\varepsilon \times d) \times 10^9] / (W \times V_2 / V_3) \times F$, where $\Delta A = \Delta A_{532} - \Delta A_{600}$; ε = molar absorption coefficient; d = colorimetric path length; V_1 = total reaction volume; V_2 = sample volume; V_3 = extract volume; W = sample mass; F = dilution factor; 10^9 = unit conversion factor (1 mol = 10^9 nmol).

Bulk segregant analysis (BSA) and sequencing

Extreme phenotypic pools were constructed from the F_2 *ds1*×Zhongmai175 population by collecting leaf tissue at the trinucleate stage from 60 plants with normal apical spikelets (WT

pool) and 60 plants with degenerated apical spikelets (mutant pool). Exome capture sequencing was performed on both parents and the two pools. The *ds1* was also subjected to whole-genome resequencing for molecular marker development. Raw reads were aligned to the Chinese Spring reference genome (IWGSC RefSeq v2.1), and SNPs across all 21 chromosomes were called and filtered to identify the candidate region for spikelet degeneration following established methods (Zhang et al., 2021a; Xiong et al., 2023).

Fine mapping and candidate gene identification

The candidate chromosome was identified by SNP density, with SNP counts tallied at 10 Mb intervals to delineate the target interval. Molecular markers were developed from homozygous SNPs for fine mapping, using 100 bp flanking sequences on each side of each SNP extracted from the Chinese Spring reference genome (IWGSC RefSeq v2.1). KASP markers were designed via the 'Design CAPS/dCAPS and KASP primer for SNP site' tool at WheatOmics 1.0 (http://202.194.139.32/), and primer specificity was verified by BLAST. FAM (5'-GAAGGTGACCAAGTTCATGCT-3') and HEX (5'-GAAGGTCGGAGTCAACGGATT-3') fluorescent adaptors were appended to the 5' ends of the two forward primers, respectively. Each KASP reaction contained 120 ng DNA template, 1× KASP Master Mix (LGC Genomics, UK), 0.6 nmol/L KASP primer premix, and 2 mmol $MgCl_2$, with fluorescence detected on a FLUOstar Omega microplate reader (BMG LABTECH, Germany).Sanger sequencing markers were similarly designed against the reference genome; PCR reactions contained 200 ng DNA, 1× Phanta Flash Master Mix Dye Plus (Vazyme Biotech, China), and 0.8 nmol/L primer premix (primer sequences in Supplemental Table 2), and each marker was genotyped across the F_2 population.

High-confidence genes within the candidate interval were amplified and sequenced to identify the causal mutation. Gene bodies and promoter regions were amplified using 2× Phanta Flash Master Mix Dye Plus (Vazyme Biotech, China) (primer sequences in Supplemental Table 8). PCR products were purified with a V-ELUTE Gel Mini Purification Kit (ZOMANBIO, China), ligated into pEASY-Blunt Zero Cloning Vector (TransGen Biotech, China), transformed into *E. coli* DH5α competent cells (Genesand Biotech, China), and individual colonies were Sanger-sequenced. Primer sequences for PCR amplification are listed in Supplemental Table 7.

Gene function analysis and verification

Functional domains were annotated using InterPro (https://www.ebi.ac.uk/interpro/search/sequence/). Protein homology searches were performed at NCBI (https://www.ncbi.nlm.nih.gov/) with thresholds of query coverage > 95%, E-value = 0, and percent identity > 70%. Phosphorylation sites were predicted with NetPhos 3.1 (https://services.healthtech.dtu.dk/services/NetPhos-3.1/) using a threshold of 0.5.

Four allelic mutants of the target gene were retrieved from the Wheat JING411 TILLING Database (https://jing411.molbreeding.com/#/query) (Xiong et al., 2023) and the Fielder mutant resource (https://mutant.tcuni.com) respectively. Two stop-gained mutants, *je0428* and *e0920*, were derived from Jing411, and the other two, *F-854* (missense) and *F-868* (stop-gained), were from Fielder. 30 seeds of each were field-grown for genotypic and phenotypic validation. Mutations were confirmed by Sanger sequencing with two technical replicates, and predicted amino acid changes were annotated accordingly. Apical spikelet degeneration and middle spikelet sterility were scored as described above. Grain-bearing spikelet rate was calculated as (grain-bearing spikelet number / total spikelet number) × 100%.

RNA sequencing and expression analysis

Apical spikelets of WT and *ds1* were collected at the floral organ primordia differentiation, tetrad, and late uninucleate stages. Each young spike was bisected at mid-length, and only the apical half was retained for RNA-seq. WT and *ds1* samples were designated WS and MS, respectively. Three biological replicates were prepared per genotype per stage, each comprising pooled tissue from 20 individuals. Total RNA was extracted with TRIzol Reagent (TIANGEN Biotech, China); 1.5 μg RNA per sample was used for library construction and sequencing (Biomarker Co., Ltd., China), and the remainder was stored at −80°C for RT-qPCR.

Reads were aligned to the Chinese Spring reference genome (IWGSC RefSeq v2.1), assembled, and quantified. Expression levels were calculated as FPKM values using StringTie with the maximum flow algorithm (Trapnell et al., 2010). Differential expression analysis was performed in DESeq2 (Love et al., 2014), with $|\text{fold change}| \geq 2$ and FDR < 0.01 as significance thresholds. Differentially expressed genes were annotated against GOC, KOC, GO, and KEGG databases, and significantly enriched terms were identified via BMKCloud (BioMarker, China). After clustering genes into modules of a gene co-expression network via WGCNA analysis, a correlation analysis was performed between these modules and spike development to screen modules highly correlated with the phenotype. The value of kME was calculated, a value closer to '1' (red) indicates a stronger positive correlation, and a value closer to '-1' (blue) indicates a stronger negative correlation.

RT-qPCR

At the trinucleate stage, apical spikelets, basal spikelets, stems and leaves were collected from WT and *ds1*, along with apical spikelets from F_3 recombinant lines derived from a cross between

ds1 and Zhongmai175 for total RNA extraction. cDNA was synthesized using HiScript IV All-in-One Ultra RT SuperMix for qPCR (Vazyme Biotech, China). Quantitative PCR was performed with Taq Pro Universal SYBR qPCR Master Mix (Vazyme Biotech, China) on a CFX96 Real-Time System (Bio-Rad, USA). *ACTIN* (*TraesCS5D03G0333200*) served as the internal reference. Three biological replicates with three technical replicates each were performed per gene. Primer sequences are provided in Supplemental Tables 9 and 10.

Acknowledgments

This study was supported by the National Key Research and Development Program (Grant No. 2022YFD1200700), China Agriculture Research System of MOF and MARA (CARS-03) and the Agricultural Science and Technology Innovation Program of P.R. China. We thank the Major Platform Center, Institute of Crop Sciences, Chinese Academy of Agricultural Sciences for their technical support in scanning electron microscope and transmission electron microscope.

Author contributions

L.L. and H.G. conceived of and designed the experiments. Q.D., Z.F., Y.X., H.X., L.Z., J.G. and H.L. performed the experiments and analyzed the data. Q.D. and H.G. wrote the article. All authors read and approved the final version of the manuscript. All authors have read and agreed to the published version of the manuscript.

Figure Legends

Figure 1. Phenotypic characterization of *ds1*.

A and B) Whole plants (A) and spikes (B) of WT and *ds1* at the grain-filling stage. **(C)** Time-course development of young spikes in WT (left) and *ds1* (right) at each developmental stage. **(D)** Spikes at the late uninucleate stage. **(E)** Spikes and florets of *ds1* at the binucleate stage. Red lines denote the spikelet positions used for sampling and length measurement in C and E. Scale bars = 15 cm in A; 1 cm in B, D, and E; 1 mm in C.

Figure 2. Anther morphology and reactive oxygen species levels in WT and *ds1*.

(A to C) Anther structure at flowering stage in WT apical spikelets (A), *ds1* middle sterile spikelets (B), and *ds1* apical degenerated spikelets (C). **(D to F)** I_2-KI-stained pollen from WT apical spikelets (D), *ds1* middle spikelet sterile anthers (E), and *ds1* apical degenerated spikelet anthers (F). **(G to J)** DAB staining showing H_2O_2 accumulation (G), NBT staining showing O_2^- accumulation (H), SOD activity (I), and MDA content (J) in WT and *ds1*. Scale bars = 1 mm in A to H. Data are means ± SD; $n = 3$ in G and H (3 biological replicates); $n = 12$ in I and J (3 biological replicates with 4 technical replicates). Statistical significance determined by two-tailed unpaired Student's *t*-test (*$P < 0.05$, **$P < 0.01$).

Figure 3. SEM analysis of anther outer surface and internal structure at the trinucleate stage.

(A to F) Anther outer wall of WT apical spikelets (A and B), *ds1* middle spikelets (C and D), and *ds1* apical spikelets (E, F). **(G to I)** Anther internal structure. **(J to L)** Pollen grains. **(M to O)** Pollen exine surface. **(P to R)** Ubisch bodies on the anther inner wall. WT, apical spikelet anthers of WT; *ds1-a*, apical spikelet anthers of *ds1*; *ds1-m*, middle spikelet anthers of *ds1*. Scale bars = 200 μm in A, C, and E; 5 μm in B, D, and F; 50 μm in G to I; 10 μm in J to L; 2 μm in M to R. Abbreviations: An, anther; DAn, degraded anther; DEX, degraded exine; DMP, degraded mature pollen; DUb, degraded Ubisch body; Ex, exine; GP, germination pore; MP, mature pollen; Ub, Ubisch body.

Figure 4. Toluidine blue-stained anther cross-sections and TEM ultrastructure across developmental stages.

(A and E) Early uninucleate stage cross-sections. **(B, F, and I)** Late uninucleate stage. **(C, G, and J)** Binucleate stage. **(D, H, and K)** Trinucleate stage. **(L to N)** TEM cross-sections at the binucleate stage. **(O to Q)** TEM cross-sections at the trinucleate stage. **(R to T)** Starch grain content at the trinucleate stage. **(U to W)** Pollen wall ultrastructure in mature pollen grains. WT, apical spikelet anthers of WT; *ds1-a*, apical spikelet anthers of *ds1*; *ds1-m*, middle spikelet anthers of *ds1*. Scale bars = 50 μm in A to K; 100 μm in L to Q; 5 μm in R to W. Abbreviations: Ba, baculum; Cy, cytoplasm; DEX, degraded exine; DMP, degraded mature pollen; DMsp, degraded microspore; E, epidermis; En, endothecium; EX, exine; In, intine; Mch, microchannel; ML, middle layer; MP, mature pollen; Msp, microspore; Ne, nexine; S, starch; T, tapetum; Te, tectum.

Figure 5. Map-based cloning and molecular characterization of *ds1* gene.

(A) Preliminary and fine mapping of *ds1* on chromosome 3B. **(B)** Expression levels of the seven genes within the candidate interval. **(C)** Tissue expression profile of the target gene. **(D and E)** Mutation site and phenotypes of allelic mutants derived from Jing411 (D) and Fielder (E) at the trinucleate stage with I_2-KI staining of middle anthers. **(F and G)** Grain-bearing spikelet number (F) and grain-bearing spikelet rate (G) in allelic mutants derived from Jing411 background. **(H and I)** Grain-bearing spikelet number (H) and grain-bearing spikelet rate (I) in allelic mutants derived from Fielder background. The brown arrow indicates a mutation site of *ds1* and orange arrows indicate the pollen source (D and E). Data are means ± SD; $n = 9$ in B and C (3 biological replicates with 3 technical replicates); $n = 10$ in F to I (10 biological replicates). Statistical significance by two-tailed unpaired Student's *t*-test ($^*P < 0.05$, $^{**}P < 0.01$).

Figure 6. Differential expression of MADS-box transcription factors in *ds1* apical spikelets.

(A) Heatmap of MADS-box gene expression across developmental stages and genotypes. **(B)** RT-qPCR quantification of selected MADS-box transcription factors. **(C)** Module-spike relationships derived from WGCNA. **(D)** Expression patterns of MADS-box genes in recombinant lines derived from the cross between *ds1* and Zhongmai175. MS-1, *ds1* apical spikelets at floral organ primordia differentiation stage; MS-3, *ds1* apical spikelets at late uninucleate stage; WS-1, WT apical spikelets at floral organ primordia differentiation stage; WS-3, WT apical spikelets at late uninucleate stage. Data are means ± SD; $n = 9$ (3 biological replicates with 3 technical replicates). Statistical significance by two-tailed unpaired Student's *t*-test ($^*P < 0.05$, $^{**}P < 0.01$).

1 **Figure 1**

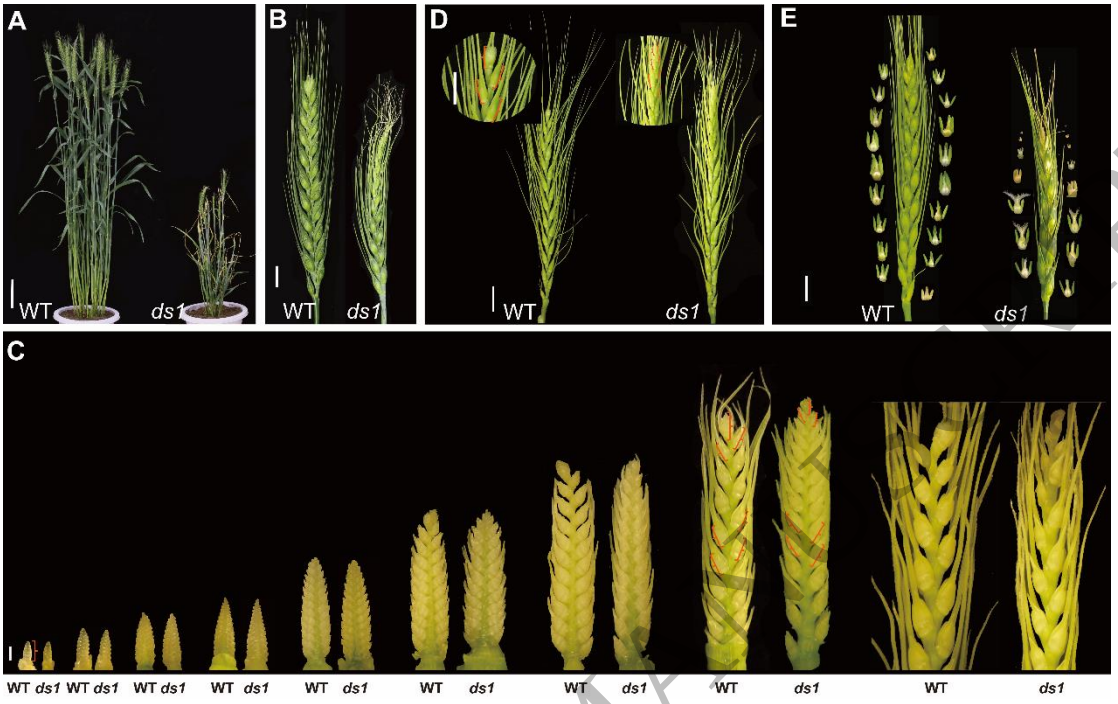

2

3

Figure 2

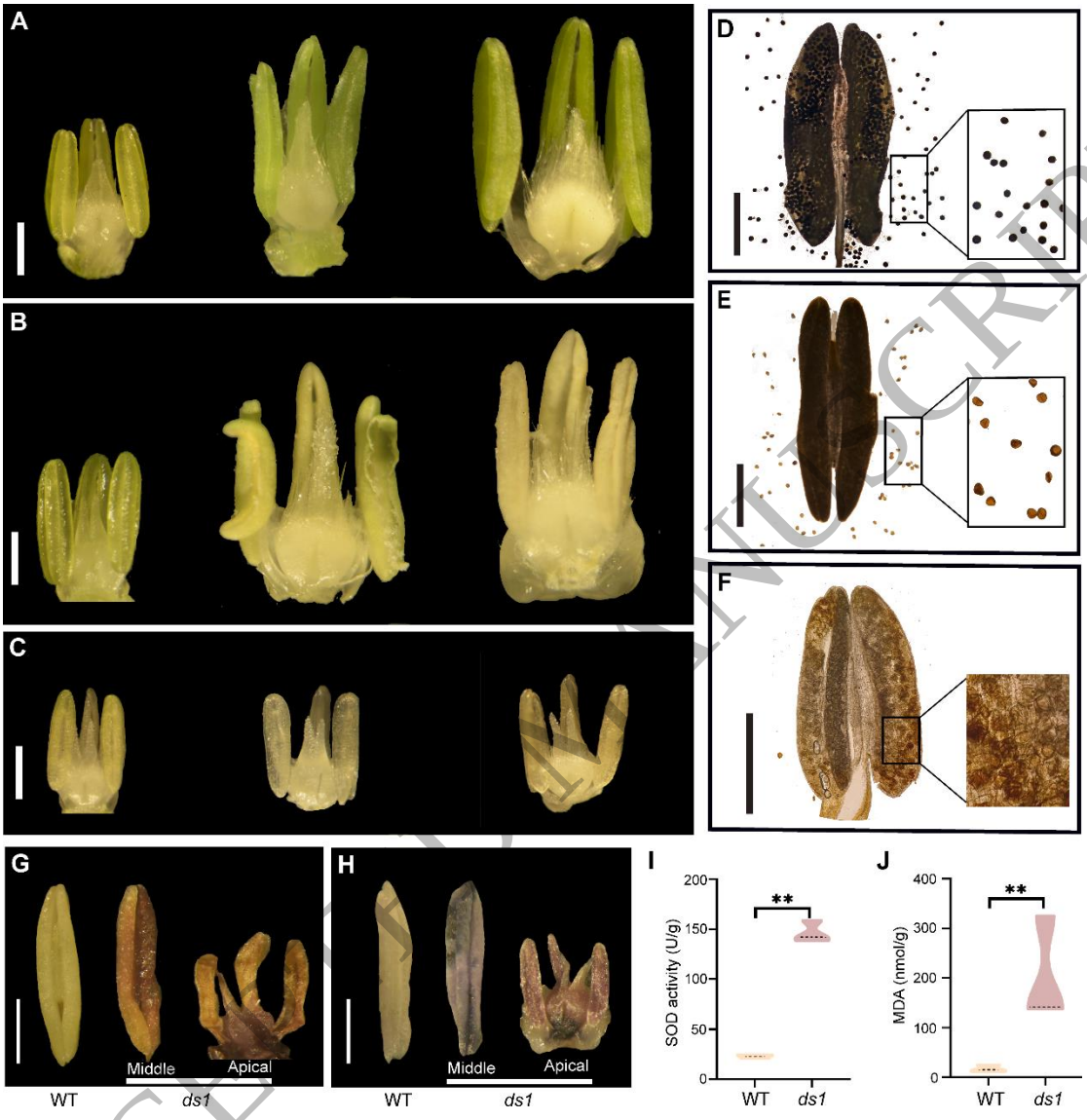

Figure 3

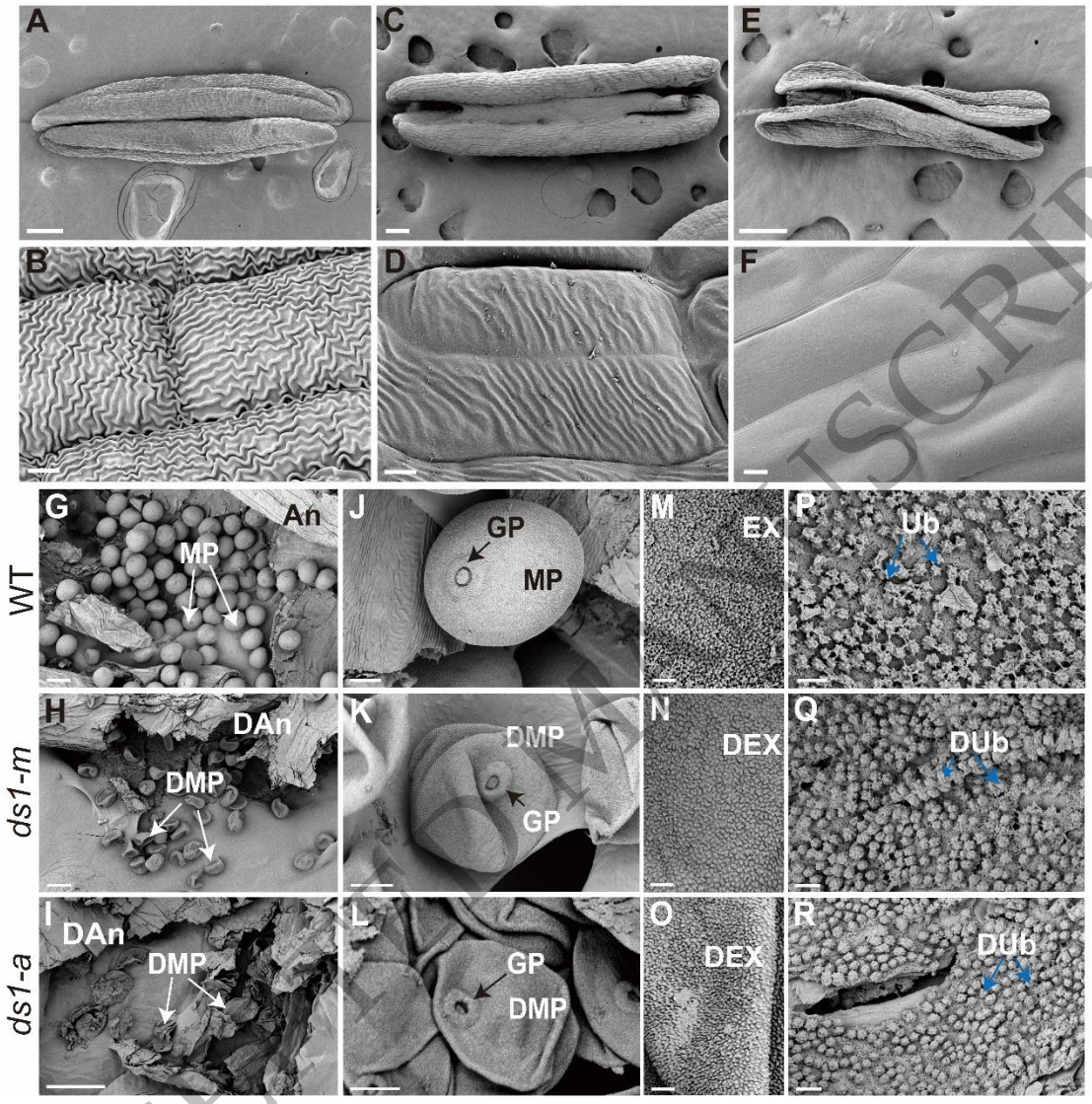

Figure 4

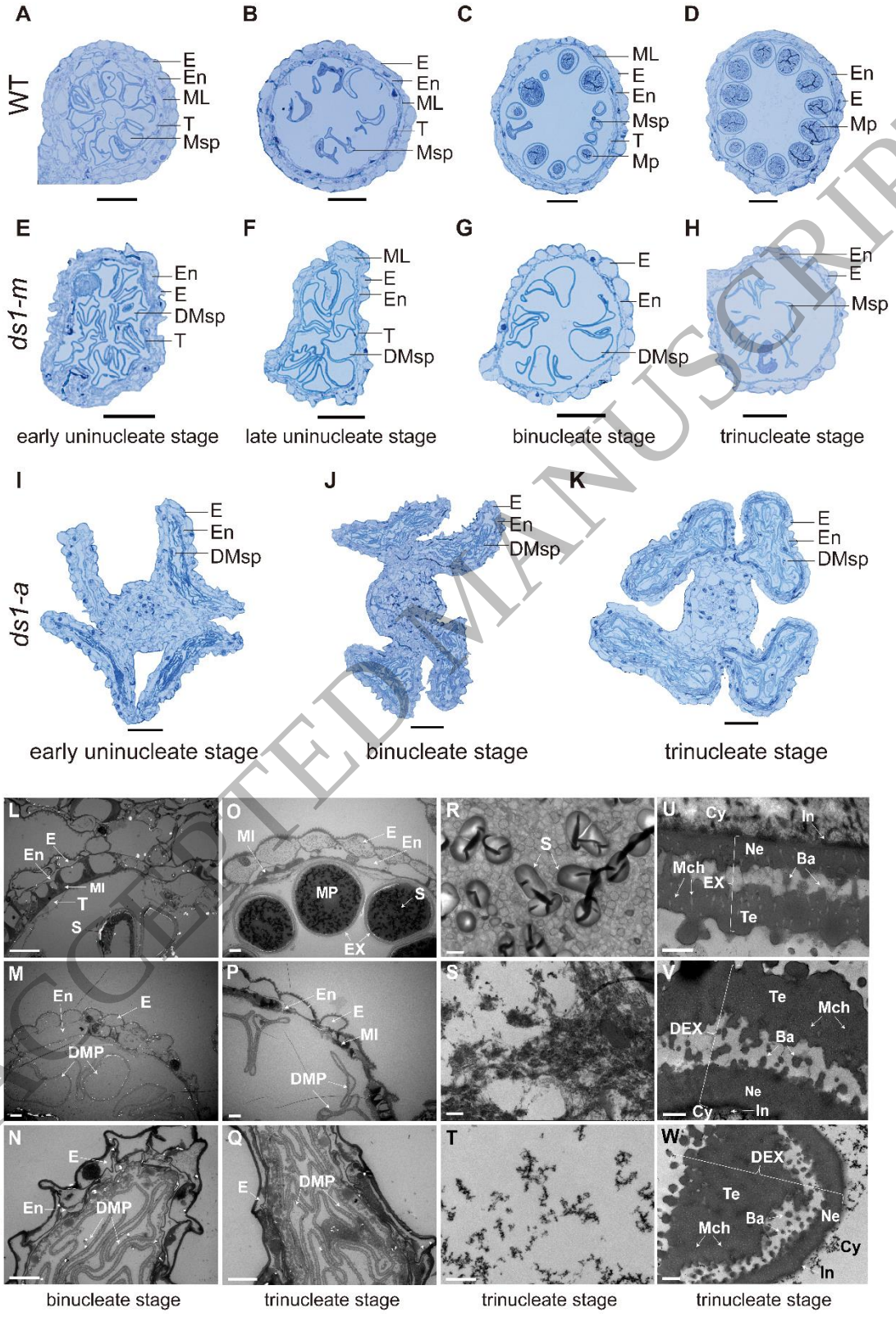

1 **Figure 5**

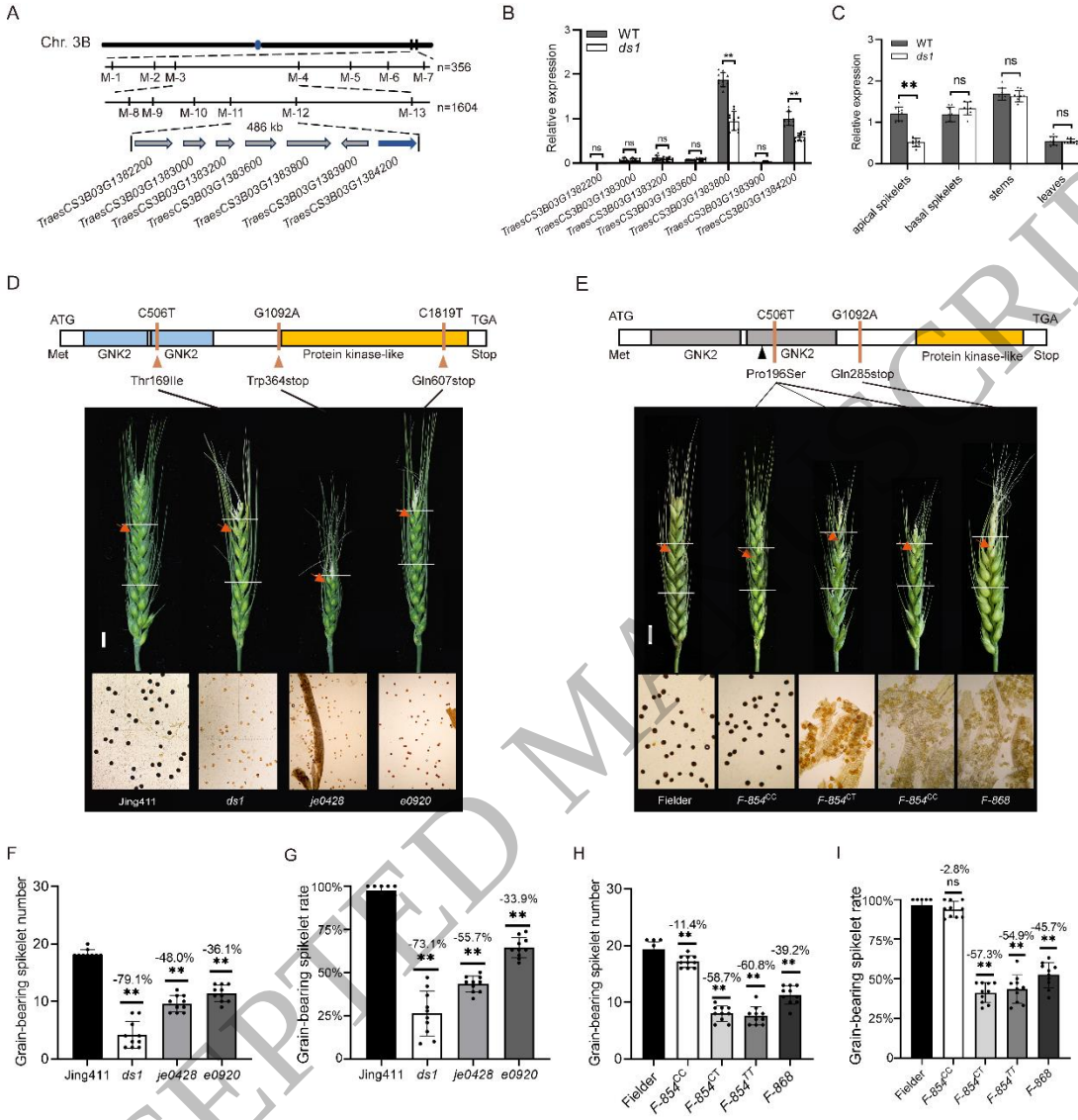

2

3

1 **Figure 6**

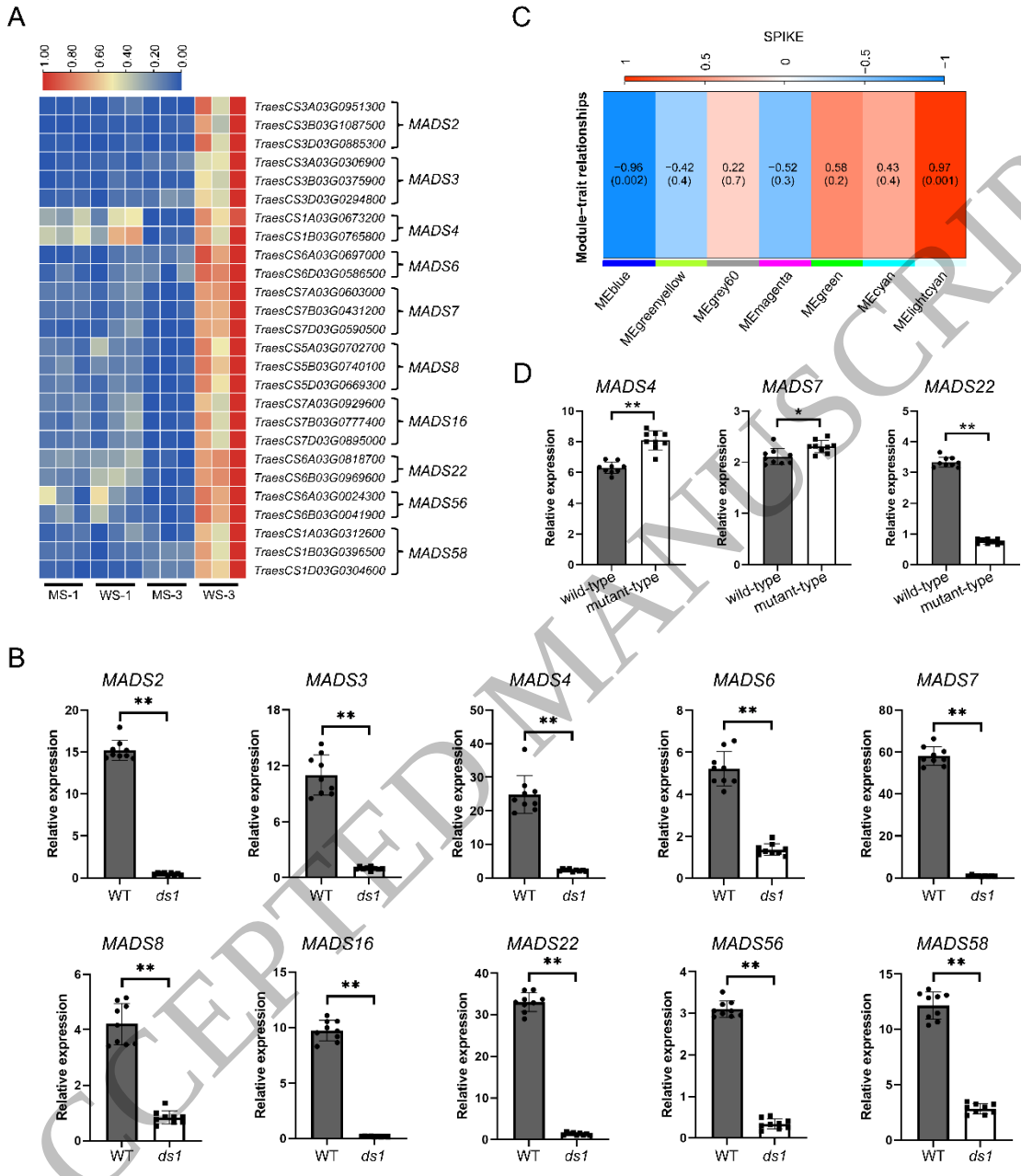

2

3

References

Albrecht C, Russinova E, Hecht V, Baaijens E and de Vries S (2005) The *Arabidopsis thaliana* SOMATIC EMBRYOGENESIS RECEPTOR-LIKE KINASES1 and 2 control male sporogenesis. The Plant Cell, 17: 3337-3349

Ali A, Wu TK, Zhang HY, Xu PZ, Zafar SA, Liao YX, Chen XQ, Zhou H, Liu YT, Wang WM and Wu XJ (2022) A putative SUBTILISIN-LIKE SERINE PROTEASE 1 (SUBSrP1) regulates anther cuticle biosynthesis and panicle development in rice. Journal of Advanced Research, 42: 273-287

An XL, Ma B, Duan MJ, Dong ZY, Liu RG, Yuan DY, Hou QC, Wu SW, Zhang DF, Liu DC, Yu D, Zhang YW, Xie K, Zhu TT, Li ZW, Zhang SM, Tian YH, Liu C, Li JP, Yuan LP and Wan XY (2020) Molecular regulation of *ZmMs7* required for maize male fertility and development of a dominant male-sterility system in multiple species. Proceedings of the National Academy of Sciences of the United States of America, 117(38): 23499-23509

Ariizumi T and Toriyama K (2011) Genetic regulation of sporopollenin synthesis and pollen exine development. Annual Review of Plant Biology, 62: 437-460

Backhaus AE, Lister A, Tomkins M, Adamski NM, Simmonds J, Macaulay I, Morris RJ, Haerty W and Uauy C (2022) High expression of the MADS-box gene *VRT2* increases the number of rudimentary basal spikelets in wheat. Plant Physiology, 189(3): 1536-1552

Bai JT, Zhu XD, Wang Q, Zhang J, Chen HQ, Dong GJ, Zhu L, Zheng HK, Xie QJ, Nian JQ, Chen F, Fu Y, Qian Q and Zuo JR (2015) Rice *TUTOU1* encodes a suppressor of cAMP receptor-like protein that is important for actin organization and panicle development. Plant Physiology, 169(2): 1179-1191

Bai WT, Wang PR, Hong J, Kong WY, Xiao YJ, Yu XW, Zheng H, You SM, Lu JY, Lei DK, Wang CL, Wang QM, Liu SJ, Liu X, Tian YL, Chen LM, Jiang L, Zhao ZG, Wu CY and Wan JM (2019) *Earlier Degraded Tapetum1* (*EDT1*) Encodes an ATP-Citrate Lyase Required for Tapetum Programmed Cell Death. Plant Physiology,181(3): 1223-1238

Bush SM and Krysan PJ (2007) Mutational evidence that the *Arabidopsis* MAP kinase MPK6 is involved in anther, inflorescence, and embryo development. Journal of Experimental Botany, 58(8): 2181-2191

Callens C, Tucker MR, Zhang DB and Wilson ZA (2018) Dissecting the role of MADS-box genes in monocot floral development and diversity. Journal of Experimental Botany, 69(10): 2435-2459

Chang ZY, Chen ZF, Yan W, Xie G, Lu JW, Wang N, Lu QQ, Yao N, Yang GZ, Xia JX and Tang XY (2016) An ABC transporter, OsABCG26, is required for anther cuticle and pollen exine formation and pollen-pistil interactions in rice. Plant Science, 253: 21-30

Chen LB, Ji CH, Zhou DG, Gou X, Tang JN, Jiang YJ, Han JL, Liu YG, Chen LT and Xie YY (2022) OsLTP47 may function in a lipid transfer relay essential for pollen wall development in rice. Journal of Genetics and Genomics, 49(5): 481-491

Chongloi GL, Prakash S and Vijayraghavan U (2019) Regulation of meristem maintenance and organ identity during rice reproductive development. Journal of Experimental Botany, 70(6): 1719-1736

Colcombet J, Boisson-Dernier A, Ros-Palau R, Vera CE and Schroeder JI (2005) *Arabidopsis* SOMATIC EMBRYOGENESIS RECEPTOR KINASES1 and 2 are essential for tapetum development and microspore maturation. The Plant Cell, 17(12): 3350-3361

Cui RF, Han JK, Zhao SZ, Su KM, Wu F, Du XQ, Xu QJ, Chong K, Theissen G and Meng Z (2010) Functional conservation and diversification of class E floral homeotic genes in rice (*Oryza sativa*). The Plant Journal, 61(5): 767-781

Du DJ, Zhang DX, Yuan J, Feng M, Li ZJ, Wang ZH, Zhang ZH, Li XT, Ke WS, Li RH, Chen ZY, Chai LL, Hu ZR, Guo WL, Xing JW, Su ZQ, Peng HR, Xin MM, Yao YY, Sun QX, Liu J and Ni ZF (2021) *FRIZZY PANICLE* defines a regulatory hub for simultaneously controlling spikelet formation and awn elongation in bread wheat. New Phytologist, 231: 814-833

Duan YL, Li SP, Chen ZW, Zheng LL, Diao ZJ, Zhou YC, Lan T, Guan HZ, Pan RS, Xue YB and Wu WR (2012) *Dwarf and deformed flower 1*, encoding an F-box protein, is critical for vegetative and floral development in rice (*Oryza sativa* L.). The Plant Journal, 72(5): 829-842

Fornara F, Gregis V, Pelucchi N, Colombo L and Kater M (2008) The rice *StMADS11*-like genes *OsMADS22* and *OsMADS47* cause floral reversions in *Arabidopsis* without complementing the *svp* and *agl24* mutants. Journal of Experimental Botany, 59(8): 2181-2190

Gómez JF, Talle B and Wilson ZA (2015) Anther and pollen development: A conserved developmental pathway. Journal of Integrative Plant Biology, 57(11): 876-891

Guo HJ, Yan ZH, Li X, Xie YD, Xiong HC, Liu YC, Zhao LS, Gu JY, Zhao SR and Liu LX (2017) Development of a High-Efficient Mutation Resource with Phenotypic Variation in Hexaploid Winter Wheat and Identification of Novel Alleles in the *TaAGP.L-B1* Gene. Frontiers in Plant Science, 8: 1404

Guo T, Lu ZQ, Shan JX, Ye WW, Dong NQ and Lin HX (2020) *ERECTA1* Acts Upstream of the OsMKKK10-OsMKK4-OsMPK6 Cascade to Control Spikelet Number by Regulating Cytokinin Metabolism in Rice. The Plant Cell, 32(9): 2763-2779

Han Y, Jiang SZ, Zhong X, Chen X, Ma CK, Yang YM, Mao YC, Zhou SD, Zhou L, Zhang YF, Huang XH, Zhang H, Li LG, Zhu J and Yang ZN (2023) Low temperature compensates for defective tapetum initiation to restore the fertility of the novel TGMS line *ostms15*. Plant Biotechnology Journal, 21(8): 1659-1670

Heng YQ, Wu CY, Long Y, Luo S, Ma J, Chen J, Liu JF, Zhang H, Ren YL, Wang M, Tan JJ, Zhu SS, Wang JL, Lei CL, Zhang X, Guo XP, Wang HY, Cheng ZJ and Wan JM (2018) OsALMT7 Maintains Panicle Size and Grain Yield in Rice by Mediating Malate Transport. The Plant Cell, 30(4): 889-906

Hord CLH, Sun YJ, Pillitterie LJ, Toriie KU, Wang HC, Zhang SQ and Ma H (2008) Regulation of *Arabidopsis* early anther development by the mitogen-activated protein kinases, MPK3 and MPK6, and the ERECTA and related receptor-like kinases. Molecular Plant, 1(4): 645-658

Hord CLH, Chen CB, Deyoung BJ, Clark SE and Ma H (2006) The BAM1/BAM2 receptor-like kinases are important regulators of *Arabidopsis* early anther development. The Plant Cell, 18(7):1667-1680

Hou QC, An XL, Ma B, Wu SW, Wei X, Yan TW, Zhou Y, Zhu TT, Xie K, Zhang DF, Li ZW, Zhao LN, Niu CF, Long Y, Liu C, Zhao W, Ni F, Li JP, Fu DL, Yan ZN and Wan XY (2023) ZmMS1/ZmLBD30-orchestrated transcriptional regulatory networks precisely control pollen exine development. Molecular Plant, 16(8): 1321-1338

Huo YQ, Pei YR, Tian YH, Zhang ZG, Li K, Liu J, Xiao SL, Chen HB and Liu J (2020) *IRREGULAR POLLEN EXINE2* Encodes a GDSL Lipase Essential for Male Fertility in Maize. Plant Physiology, 184(3): 1438-1454

Ji CH, Li HY, Chen LB, Xie M, Wang FP, Chen YL and Liu YG (2013) A Novel Rice bHLH Transcription Factor, DTD, Acts Coordinately with TDR in Controlling Tapetum Function and Pollen Development. Molecular Plant, 6(5): 1715-1718

Jia GX, Liu XD, Owen HA and Zhao DZ (2008) Signaling of cell fate determination by the TPD1 small protein and EMS1 receptor kinase. Proceedings of the National Academy of Sciences of the United States of America, 105(6): 2220-2225

Ko SS, Li MJ, Ku MSB, Ho YC, Lin YJ, Chuang MH, Hsing HX, Lien YC, Yang HT, Chang HC and Chan MT (2014) The bHLH142 Transcription Factor Coordinates with TDR1 to Modulate the Expression of *EAT1* and Regulate Pollen Development in Rice. The Plant Cell, 26(6): 2486-2504

Kong XC, Wang F, Geng SF, Guan JT, Tao S, Jia ML, Sun GL, Wang ZY, Wang K, Ye XG, Ma J, Liu DC, Wei YM, Zheng YL, Fu XD, Mao L, Lan XJ and Li AL (2022) The wheat *AGL6*-like MADS-box gene is a master regulator for floral organ identity and a target for spikelet meristem development manipulation. Plant Biotechnology Journal, 20(1): 75-88

Kouidri A, Baumann U, Okada T, Baes M, Tucker EJ and Whitford R (2018) Wheat TaMs1 is a glycosylphosphatidylinositol-anchored lipid transfer protein necessary for pollen development. BMC Plant Biology, 18: 332

Lee SH, Jung KH, An GH and Chung YY (2004) Isolation and Characterization of a Rice Cysteine Protease Gene, *OsCP1*, Using T-DNA Gene-Trap System. Plant Molecular Biology, 54(5): 755-765

Lee SY, Choi SC and An GH (2008) Rice SVP-group MADS-box proteins, OsMADS22 and OsMADS55, are negative regulators of brassinosteroid responses. The Plant Journal, 54(1): 93-105

Li CX, Lin HQ, Chen A, Lau MY, Jernstedt J and Dubcovsky J (2019) Wheat *VRN1*, *FUL2* and *FUL3* play critical and redundant roles in spikelet development and spike determinacy. Development, 146(14): dev175398

Li H, Yuan Z, Vizcay-Barrena G, Yang CY, Liang WQ, Zong J, Wilson ZA and Zhang DB (2011) *PERSISTENT TAPETAL CELL1* Encodes a PHD-Finger Protein That Is Required for Tapetal Cell Death and Pollen Development in Rice. Plant Physiology, 156(2): 615-630

Li K, Debernardi JM, Li CX, Lin HQ, Zhang CZ, Jernstedt J, Korff MV, Zhong JS and Dubcovsky J (2021) Interactions between SQUAMOSA and SHORT VEGETATIVE PHASE MADS-box proteins regulate meristem transitions during wheat spike development. The Plant Cell, 33(12): 3621-3644

Li N, Zhang DS, Liu HS, Yin CS, Li XX, Liang WQ, Yuan Z, Xu B, Chu HW, Wang J, Wen TQ, Huang H, Luo D, Ma H and Zhang DB (2006) The Rice *Tapetum Degeneration Retardation* Gene Is Required for Tapetum Degradation and Anther Development. The Plant Cell, 18(11): 2999-3014

Li YP, Li L, Zhao MC, Guo L, Guo XX, Zhao D, Batool A, Dong BD, Xu HX, Cui SJ, Zhang AM, Fu XD, Li JM, Jing RL and Liu XG (2020) Wheat *FRIZZY PANICLE* activates *VERNALIZATION1-A* and *HOMEOBOX4-A* to regulate spike development in wheat. Plant Biotechnology Journal, 19(6): 1141-1154

Liu J, Xia C, Dong HX, Liu P, Yang RZ, Zhang LC, Liu X, Jia JZ, Kong XY and Sun JQ (2022a) Wheat Male sterile 2 reduces the ROS levels to inhibit anther development by deactivating ROS modulator 1. Molecular Plant, 15(9):1428-1439

Liu JL, Ye Q, Jiang WX, Liu SQ, Wu Z, Hu XF, Wang XQ, Zhang ZL, Guo DD, Chen XR, He HH and Hu LF (2024) *Abnormal Degraded Tapetum 1* (*ADT1*) is required for tapetal cell death and pollen development in rice. Theoretical and Applied Genetics, 137(7): 170

Liu SS, Li ZW, Wu SW and Wan XY (2021a) The essential roles of sugar metabolism for pollen development and male fertility in plants. The Crop Journal, 9: 1223-1236

Liu T, Jiang GQ, Yao XF and Liu CM (2021b) The leucine-rich repeat receptor-like kinase OsERL plays a critical role in anther lobe formation in rice. Biochemical and Biophysical Research Communications, 563: 85-91

Liu XZ, Jiang YL, Wu SW, Wang J, Fang CW, Zhang SW, Xie RR, Zhao LN, An XL, and Wan XY (2022b) The ZmMYB84-*ZmPKSB* regulatory module controls male fertility through modulating anther cuticle - pollen exine trade-off in maize anthers. Plant Biotechnology Journal, 20(12): 2342-2356

Love MI, Huber W and Anders S (2014) Moderated estimation of fold change and dispersion for RNA-seq data with DESeq2. Genome Biology, 15(12): 550

Ma K, Han JL, Zhang ZX, Li HY, Zhao YC, Zhu QL, Xie YY, Liu YG and Chen LT (2021) OsEDM2L mediates m^{6}A of *EAT1* transcript for proper alternative splicing and polyadenylation regulating rice tapetal degradation. Journal of Integrative Plant Biology, 63(11): 1982-1994

Ni F, Qi J, Hao QQ, Lyu B, Luo MC, Wang Y, Chen FJ, Wang SY, Zhang CZ, Epstein L, Zhao XY, Wang HG, Zhang XS, Chen CX, Sun LZ and Fu DL (2017) Wheat *Ms2* encodes for an orphan protein that confers male sterility in grass species. Nature Communications, 8: 15121

Niu NN, Liang WQ, Yang XJ, Jin WL, Wilson ZA, Hu JP and Zhang DB (2013) EAT1 promotes tapetal cell death by regulating aspartic proteases during male reproductive development in rice. Nature Communications, 4: 1445

Nonomura KI, Miyoshi K, Eiguchi M, Suzuki T, Miyao A, Hirochika H and Kurata N (2003) The *MSP1* Gene Is Necessary to Restrict the Number of Cells Entering into Male and Female Sporogenesis and to Initiate Anther Wall Formation in Rice. The Plant Cell, 15(8): 1728-1740

Peng YB, Hou FX, Bai Q, Xu PZ, Liao YX, Zhang HY, Gu CJ, Deng XS, Wu TK, Chen XQ, Ali A and Wu XJ (2018) Rice Calcineurin B-Like Protein-Interacting Protein Kinase 31 (OsCIPK31) is Involved in the Development of Panicle Apical Spikelets. Frontiers in Plant Science, 9: 1661

Piovesana M, Wood AKM, Smith DP, Deery MJ, Bayliss R, Carrera E, Wellner N, Kosik O, Napier JA, Kurup S and Matthes MC (2023) A point mutation in the kinase domain of CRK10 leads to xylem vessel collapse and activation of defence responses in Arabidopsis. Journal of Experimental Botany, 74(10): 3104-3121

Qin P, Tu B, Wang YP, Deng LC, Quilichini TD, Li T, Wang H, Ma BT and Li SG (2013) *ABCG15* encodes an ABC transporter protein, and is essential for post-meiotic anther and pollen exine development in rice. Plant and Cell Physiology, 54(1):138-154

Schilling S, Kennedy A, Pan S, Jermiin LS and Melzer R (2020) Genome-wide analysis of MIKC-type MADS-box genes in wheat: pervasive duplications, functional conservation and putative neofunctionalization. New Phytologist, 225(1): 511-529

Sentoku N, Kato H, Kitano H and Imai R (2005) *OsMADS22*, an *STMADS11*-like MADS-box gene of rice, is expressed in non-vegetative tissues and its ectopic expression induces spikelet meristem indeterminacy. Molecular Genetics and Genomics, 273(1): 1-9

Shen H, Zhong XB, Zhao FF, Wang YM, Yan BX, Li Q, Chen GY, Mao BZ, Wang JJ, Li YS, Xiao GY, He YK, Xiao H, Li JM and He ZH (2015) Overexpression of receptor-like kinase *ERECTA* improves thermotolerance in rice and tomato. Nature Biotechnology, 33(9): 996-1003

Shen LP, Zhang LL, Yin CB, Xu XW, Liu YY, Shen KC, Wu H, Sun ZW, Wang K, He ZH, Zhang XY, Hao CY, Hou J, Bi AY, Zhao XB, Xu DX, Ye BT, Yu XC, Wang ZY, Liu DN, Hao YF, Lu F and Guo ZF (2024) The wheat sucrose synthase gene *TaSus1* is a determinant of grain number per spike. The Crop Journal, 12(1): 295-300

Shi JX, Cui MH, Yang L, Kim YJ and Zhan DB (2015) Genetic and Biochemical Mechanisms of Pollen Wall Development. Trends in Plant Science, 20(11): 741-753.

Sun M, Jiang CC, Gao GQ, An CD, Wu WX, Kan JH, Zhang JP, Li LH and Yang P (2024) A novel type of malformed floral organs mutant in barley was conferred by loss-of-function mutations of the MADS-box gene *HvAGL6*. The Plant Journal, 119(6): 2609-2621

Suzaki T, Sato M, Ashikari M, Miyoshi M, Nagato Y and Hirano HY (2004) The gene *FLORAL ORGAN NUMBER1* regulates floral meristem size in rice and encodes a leucine-rich repeat receptor kinase orthologous to *Arabidopsis* CLAVATA1. Development, 131(22): 5649-5657

Tao Y, Zou T, Zhang X, Liu R, Chen H, Yuan GQ, Zhou D, Xiong PP, He ZY, Li GW, Zhou ML, Liu SJ, Deng QM, Wang SQ, Zhu J, Liang YY, Yu XM, Zheng AP, Wang AJ, Liu HN, Wang LX, Li P and Li SC (2021) Secretory lipid transfer protein OsLTPL94 acts as a target of EAT1 and is required for rice pollen wall development. The Plant Journal, 108(2): 358-377

Tian SQ, Niu JQ, Shang QS, Wang MC, Li Y, Ji J, Wang F, Ling HQ and Si YQ (2025) Structure variation-driven activation of *TaWUS-D1* confers tri-pistil trait in wheat. Plant Communications, onlion

Trapnell C, Williams BA, Pertea G, Mortazavi A, Kwan Go, Baren MJV, Salzberg SL, Wold BJ and Pachter L (2010) Transcript assembly and quantification by RNA Seq reveals unannotated transcripts and isoform switching during cell differentiation. Nature Biotechnology, 28(5): 511-515

Tucker EJ, Baumann U, Kouidri A, Suchecki R, Baes M, Garcia M, Okada T, Dong CM, Wu YZ, Sandhu A, Singh M, Langridge P, Wolters P, Albertsen MC, Cigan AM and Whitford R (2017) Molecular identification of the wheat male fertility gene *Ms1* and its prospects for hybrid breeding. Nature Communications, 8(1): 869

Wang HQ, Sun J, Ren H, Zhao B, Ren BZ, Zhang JW, Zhang ZS, Li YT, Chen YL, Kuzyakov Y and Liu P (2025) Inhibiting reactive oxygen species production mitigates endoplasmic reticulum damage in florets of developing maize ears under heat stress. The Plant Journal, 122(5): e70243

Wang JH, Wang JJ, Li J, Shang HS, Chen XM and Hu XP (2021) The RLK protein TaCRK10 activates wheat high-temperature seedling-plant resistance to stripe rust through interacting with TaH2A.1. The Plant Journal, 108(5):1241-1255

Wang QL, Sun AZ, Chen ST, Chen LS and Guo FQ (2018) SPL6 represses signaling outputs of ER stress in control of panicle cell death in rice. Nature Plants, 4(5): 280-288.

Xie HT, Wan ZY, Li S and Zhang Y (2014) Spatiotemporal production of reactive oxygen species by NADPH oxidase is critical for tapetal programmed cell death and pollen development in *Arabidopsis*. The Plant Cell, 26(5): 2007-2023

Xiong HC, Guo HJ, Fu MY, Xie YD, Zhao LS, Gu JY, Zhao SR, Ding YP, Du QD, Zhang JZ, Qiu L, Xie XM, Zhou LB, Chen ZX and Liu LX (2023) A large‐scale whole‐exome sequencing mutant resource for functional genomics in wheat. Plant Biotechnology Journal, 21(10): 2047-2056

Xu J, Ding ZW, Vizcay-Barrena G, Shi JX, Liang WQ, Yuan Z, Werck-Reichhart D, Schreiber L, Wilson ZA and Zhang DB (2014) *ABORTED MICROSPORES* acts as a master regulator of pollen wall formation in *Arabidopsis*. The Plant Cell, 26(4): 1544-1556

Yan Q, Pang YL, Lu Y, Zhu HQ, Lu Y, Li JY, Sun ZN, Li ZY, Zhao HL, Li GY, Wu YY and Liu SB (2025) *qSL2B*/*TaeEF1A* regulates spike development and grain number in wheat. The Crop Journal, 13(3): 900-908

Yang L, Qian XL, Chen MJ, Fei QL, Meyers BC, Liang WQ and Zhang DB (2016) Regulatory Role of a Receptor-Like Kinase in Specifying Anther Cell Identity. Plant Physiology, 171(3): 2085-2100

Yang SL, Jiang LX, Puah CS, Xie LF, Zhang XQ, Chen LQ, Yang WC and Ye D (2005) Overexpression of *TAPETUM DETERMINANT1* Alters the Cell Fates in the Arabidopsis Carpel and Tapetum via Genetic Interaction with *EXCESS MICROSPOROCYTES1/EXTRA SPOROGENOUS CELLS*. Plant Physiology, 139(1): 186-191

Yang SL, Xie LF, Mao HZ, Puah CS, Yang WC, Jiang L, Sundaresan V and Ye D (2003) *TAPETUM DETERMINANT1* is required for cell specialization in the Arabidopsis anther. The Plant Cell, 15(12): 2792-2804

Yang ZF, Liu L, Sun LP, Yu P, Zhang PP, Abbas A, Xiang XJ, Wu WX, Zhang YX, Cao LY and Cheng SH (2019) *OsMS1* functions as a transcriptional activator to regulate programmed

tapetum development and pollen exine formation in rice. Plant Molecular Biology, 99: 175-191

Yao SG, Ohmori S, Kimizu M and Yoshida H (2008) Unequal Genetic Redundancy of Rice *PISTILLATA* Orthologs, *OsMADS2* and *OsMADS4*, in Lodicule and Stamen Development. Plant and Cell Physiology, 49(5): 853-857

Yi JK, Moon S, Lee YS, Zhu L, Liang WQ, Zhang DB, Jung KH, An GH (2016) Defective Tapetum Cell Death 1 (DTC1) Regulates ROS Levels by Binding to Metallothionein during Tapetum Degeneration. Plant Physiology, 170(3): 1611-1623

Yuan GQ, Zou T, He Z, Xiao Q, Li GW, Liu SJ, Xiong PP, Chen H, Peng K, Zhang X, Luo TT, Zhou D, Yang SY, Zhou FX, Zhang KX, Zheng KY, Han YH, Zhu J, Liang YY, Deng QM, Wang SQ, Sun CH, Yu XM, Liu HN, Wang LX, Li P and Li SC (2022) *SWOLLEN TAPETUM AND STERILITY 1* is required for tapetum degeneration and pollen wall formation in rice. Plant Physiology, 190(1): 352-370

Zafar SA, Patil SB, Uzair M, Fang JJ, Zhao JF, Guo TT, Yuan SJ, Uzair M, Luo Q, Shi JX, Schreiber L and Li XY (2020) *DEGENERATED PANICLE AND PARTIAL STERILITY 1* (*DPS1*) encodes a cystathionine b-synthase domain containing protein required for anther cuticle and panicle development in rice. New Phytologist, 225(1): 356-375

Zeng JG, Duan MM, Wang YQ, Li GT, You YJ, Shi J, Liu CH, Zhang JY, Xu J, Zhang SQ and Zhao J (2024) Sporophytic control of tapetal development and pollen fertility by a mitogen-activated protein kinase cascade in rice. Journal of Integrative Plant Biology, 66(7): 1500-1516

Zhan SW, An XL, Jian YL, Hou QC, Ma B, Jiang QP, Zhang K, Zhao LN and Wan XY (2024) Plastid-localized ZmENR1/ZmHAD1 complex ensures maize pollen and anther development through regulating lipid and ROS metabolism. Nature Communications, 15(1): 10857

Zhang DS, Liang WQ, Yin CS, Zong J, Gu FW and Zhang DB (2010) *OsC6*, Encoding a Lipid Transfer Protein, Is Required for Postmeiotic Anther Development in Rice. Plant Physiology, 154(1): 149-162

Zhang H, Xu H, Feng MJ and Zhu Y (2018) Suppression of *OsMADS7* in rice endosperm stabilizes amylose content under high temperature stress. Plant Biotechnology Journal, 16(1): 18-26

Zhang HH, Wang ML, Li YQ, Yan W, Chang ZY, Ni HL, Chen ZF, Wu JX, Xu CJ, Deng XW and Tang XY (2020) GDSL esterase/lipases OsGELP34 and OsGELP110/OsGELP115 are essential for rice pollen development. Journal of Integrative Plant Biology, 62(10): 1574-1593

Zhang JY, Tang YY, Pu X, Qiu XB, Wang JH, Li T, Yang Z, Zhou Y, Chang YX, Liang JJ, Zhang HL, Deng GB and Long H (2022a) Genetic and transcriptomic dissection of an artificially

induced paired spikelets mutant of wheat (*Triticum aestivum* L.). Theoretical and Applied Genetics, 135(7): 2543-2554

Zhang LC, Dong CH, Chen ZX, Gui LX, Chen C, Li DP, Xie ZC, Zhang Q, Zhang XY, Xia C, Liu X, Kong XY and Wang JR (2021a) WheatGmap: a comprehensive platform for wheat gene mapping and genomic studies. Molecular Plant, 14(2): 187-190

Zhang WD, Li HJ, Xue FY and Liang WQ (2021b) Rice Glucose 6-Phosphate/Phosphate Translocator 1 is required for tapetum function and pollen development. The Crop Journal, 9(6): 1278-1290

Zhang XY, Jia HY, Li T, Wu JZ, Nagarajan R, Lei L, Powers C, Kan CC, Hua W, Liu ZY, Chen C, Carver BF and Yan LL (2022b) *TaCol-B5* modifies spike architecture and enhances grain yield in wheat. Science, 376(6589): 180-183

Zhang YX, Tian HD, Chen D, Zhang H, Sun MH, Chen SX, Qin Z, Ding ZJ and Dai SJ (2023) Cysteine-rich receptor-like protein kinases: emerging regulators of plant stress responses. Trends in Plant Science, 28(7): 776-794

Zhao GC, Shi JX, Liang WQ, Xue FY, Luo Q, Zhu L, Qu GR, Chen MJ, Schreiber L and Zhang DB (2015) Two ATP Binding Cassette G Transporters, Rice ATP Binding Cassette G26 and ATP Binding Cassette G15, Collaboratively Regulate Rice Male Reproduction. Plant Physiology, 169(3): 2064-2079

Zhao J, Long T, Wang YF, Tong XH, Tang J, Li JL, Wang HM, Tang LQ, Li ZY, Shu YZ, Liu XX, Li SF, Liu H, Li JL, Wu YZ and Zhang J (2020) *RMS2* Encoding a GDSL Lipase Mediates Lipid Homeostasis in Anthers to Determine Rice Male Fertility. Plant Physiology, 182(4): 2047-2064

Zhou Q, Zhu J, Cui YL and Yang ZN (2015) Ultrastructure analysis reveals sporopollenin deposition and nexine formation at early stage of pollen wall development in Arabidopsis. Science Bulletin, 60(2): 273-276

Zhu L, Li F, Xie TL, Li ZW, Tian T, An XL, Wei X, Long Y, Jiao ZW and Wan XY (2024) Receptor-like kinases and their signaling cascades for plant male fertility: loyal messengers. New Phytologist, 241(4): 1421-1434